

Entangling Two Bosonic Polaritons via Dispersive Coupling with a Third Mode

Xuan Zuo,¹ Zhi-Yuan Fan,¹ Hang Qian,¹ Rui-Chang Shen,¹ and Jie Li^{1,*}

¹*Interdisciplinary Center of Quantum Information, State Key Laboratory of Modern Optical Instrumentation, and Zhejiang Province Key Laboratory of Quantum Technology and Device, School of Physics, Zhejiang University, Hangzhou 310027, China*

We provide a general mechanism of entangling two strongly-coupled bosonic systems that form two hybridized (polariton) modes. This is realized by dispersively coupling with a third bosonic mode. Stationary entanglement is achieved when the two hybridized modes are respectively resonant with the sidebands of the drive field scattered by the third mode and when the weights of the two bosonic modes in the two polaritons are appropriately chosen. The entanglement is robust against dissipations of the system and bath temperature. The entanglement theory is quite general and applicable to a variety of bosonic systems, such as cavity magnomechanical, exciton-optomechanics, and plasmon-photon-phonon systems.

Introduction.—Entangled states of bosonic systems, e.g., entangled optical and microwave fields, find a wide range of applications in quantum information science, such as quantum teleportation [1], quantum networks [2], quantum metrology [3], quantum dense coding [4] and quantum cryptography [5, 6]. Apart from entangled photons, the entanglement of other bosonic systems, e.g., vibration phonons [7, 8] and magnons [9, 10], is of particular fundamental interest in the study of macroscopic quantum states [11, 12]. Therefore, the generation of bosonic entanglement is of significant importance in the aforementioned applied and fundamental researches.

Here we provide a theory of entangling two bosonic systems that are strongly coupled, thus forming two hybridized modes. These can be cavity-magnon [13–15], exciton-photon [16–18], plasmon-photon [19], plasmon-exciton [20–23] polaritons, etc. Typically, the two hybridized modes are not entangled due to the linear excitation-exchange (beam-splitter-type) interaction between the two bosonic modes. In this Letter, we show that by introducing a third bosonic mode that is *dispersively* coupled to one of the two strongly-coupled bosonic modes, the two hybridized or polariton modes can be entangled in a stationary state. The third mode is used to introduce the parametric down-conversion (PDC) (state-swap) interaction associated with the lower (higher)-frequency polariton mode. By appropriately adjusting the strengths of the PDC and the state-swap interactions, the two polariton modes get entangled via the mediation of the third mode. The entanglement mechanism is designed for strongly-coupled bosonic systems, and is general in that it can be applied to many different kinds of bosonic systems.

The model.—The system under study consists of two continuous-variable bosonic modes, which are nearly resonant and strongly coupled forming two hybridized (polariton) modes. The strong coupling leads to the normal-mode splitting, as has been experimentally observed in a variety of systems [13–23]. One of the hybridized modes further couples to a third bosonic mode via a dispersive interaction. This is typically the situation where the resonance frequency of the third mode is much lower than the two hybridized modes. The system then becomes a hybrid system containing three bosonic modes, as depicted in Fig. 1(a). The Hamiltonian of the sys-

tem reads

$$H/\hbar = \omega_a a^\dagger a + \omega_c c^\dagger c + \omega_b b^\dagger b + G_0 c^\dagger c (b + b^\dagger) + g (a^\dagger c + a c^\dagger) + i\Omega (c^\dagger e^{-i\omega_0 t} - c e^{i\omega_0 t}), \quad (1)$$

where j (j^\dagger , $j = a, c, b$) are the annihilation (creation) operators of the three modes, respectively, satisfying the commutation relation $[j, j^\dagger] = 1$. ω_j are their corresponding resonance frequencies, and $\omega_b \ll \omega_a, \omega_c$. g denotes the coupling strength of the two strongly-coupled modes (a and c). Since the frequencies of the two modes are close, their coupling can be strong and takes a beam-splitter form, responsible for exchanging their excitations [13–23]. G_0 is the single-excitation dispersive coupling strength between the lower-frequency mode b and the mode c (or a). Such a Hamiltonian (1) with both linear and dispersive couplings can describe the interactions of many bosonic systems, e.g., cavity magnomechanical [9, 24–26] and exciton-optomechanics sys-

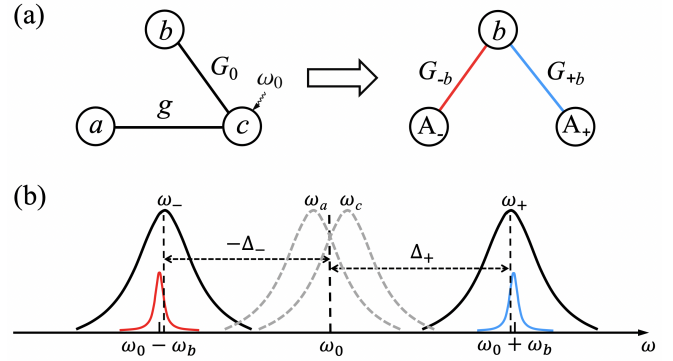


FIG. 1: (a) The three-body bosonic system. The mode c couples to the mode a via a beam-splitter interaction and to the mode b via a dispersive interaction. Two strongly-coupled modes a and c form two hybridized (polariton) modes A_- and A_+ , of which both are coupled to the mode b . (b) Frequencies and linewidths of the system. The mode c at frequency ω_c is strongly driven by a bosonic field at frequency ω_0 , and the mode b at frequency ω_b scatters the driving bosons onto the Stokes sideband at $\omega_0 - \omega_b$ and the anti-Stokes sideband at $\omega_0 + \omega_b$. When the frequencies of the two polaritons match the two sidebands, the two polariton modes are entangled via the mediation of the mode b .

tems [27–29]. Due to the dispersive nature, the bare coupling G_0 is typically weak, but its effective coupling G can be significantly improved by applying a strong drive field (at frequency ω_0) onto the mode c , with Ω being the corresponding mode-drive coupling strength.

When the modes a and c are strongly coupled and thus hybridized, it is more convenient to describe the system with the polariton operators A_{\pm} . The Hamiltonian (1) can then be rewritten in terms of A_{\pm} and, in the interaction picture with respect to $\hbar\omega_0(A_+^\dagger A_+ + A_-^\dagger A_-)$, is given by [30]

$$H/\hbar = \Delta_+ A_+^\dagger A_+ + \Delta_- A_-^\dagger A_- + \omega_b b^\dagger b + G_0 (b + b^\dagger) \times \left[A_+^\dagger A_+ \sin^2 \theta + A_-^\dagger A_- \cos^2 \theta + \frac{1}{2} (A_+^\dagger A_- + A_-^\dagger A_+) \sin 2\theta \right] + i\Omega (A_+^\dagger \sin \theta + A_-^\dagger \cos \theta - A_+ \sin \theta - A_- \cos \theta), \quad (2)$$

where A_+ and A_- are the annihilation operators of the two polariton modes, which are the hybridization of the modes a and c , via $A_+ = a \cos \theta + c \sin \theta$ and $A_- = -a \sin \theta + c \cos \theta$, with $\theta = \frac{1}{2} \arctan \frac{2g}{\omega_a - \omega_c}$. A_{\pm} satisfy the bosonic commutation relation $[k, k^\dagger] = 1$ ($k = A_{\pm}$). $\Delta_{\pm} = \omega_{\pm} - \omega_0$ denote the polariton-drive detunings, where $\omega_{\pm} = \frac{1}{2} [\omega_a + \omega_c \pm \sqrt{(\omega_a - \omega_c)^2 + 4g^2}]$ are the frequencies of the polaritons; see Fig. 1(b).

By including the dissipation and input noise of each mode, we obtain the following quantum Langevin equations (QLEs) of the system [30]:

$$\begin{aligned} \dot{A}_+ &= -i\Delta_+ A_+ - iG_0 (b + b^\dagger) (A_+ \sin^2 \theta + A_- \sin \theta \cos \theta) - \kappa_+ A_+ - \delta\kappa A_- + \Omega \sin \theta + \sqrt{2\kappa_+} A_+^{in}, \\ \dot{A}_- &= -i\Delta_- A_- - iG_0 (b + b^\dagger) (A_- \cos^2 \theta + A_+ \cos \theta \sin \theta) - \kappa_- A_- - \delta\kappa A_+ + \Omega \cos \theta + \sqrt{2\kappa_-} A_-^{in}, \\ \dot{b} &= -i\omega_b b - iG_0 (A_+^\dagger A_+ \sin^2 \theta + A_-^\dagger A_- \sin \theta \cos \theta + A_-^\dagger A_+ \cos \theta \sin \theta + A_+^\dagger A_- \cos^2 \theta) - \kappa_b b + \sqrt{2\kappa_b} b^{in}, \end{aligned} \quad (3)$$

where $\kappa_+ \equiv \kappa_a \cos^2 \theta + \kappa_c \sin^2 \theta$ and $\kappa_- \equiv \kappa_a \sin^2 \theta + \kappa_c \cos^2 \theta$ are the dissipation rates of the two polariton modes A_+ and A_- , respectively, and $\delta\kappa \equiv (\kappa_c - \kappa_a) \sin \theta \cos \theta$ denotes the coupling strength between the two polaritons due to the unbalanced dissipation rates $\kappa_a \neq \kappa_c$, with κ_j being the dissipation rate of the mode j ($j = a, c, b$). $A_+^{in} \equiv (\sqrt{2\kappa_a} \cos \theta a^{in} + \sqrt{2\kappa_c} \sin \theta c^{in})/\sqrt{2\kappa_+}$ and $A_-^{in} \equiv (-\sqrt{2\kappa_a} \sin \theta a^{in} + \sqrt{2\kappa_c} \cos \theta c^{in})/\sqrt{2\kappa_-}$ represent the noises entering the two polariton modes, which are related to the input noises a^{in} , c^{in} of the modes a and c . b^{in} is the input noise of the mode b . $j^{in}(t)$ ($j = a, c, b$) are zero-mean and characterized by the correlation functions [31]: $\langle j^{in}(t) j^{in\dagger}(t') \rangle = [N_j(\omega_j) + 1] \delta(t - t')$, $\langle j^{in\dagger}(t) j^{in}(t') \rangle = N_j(\omega_j) \delta(t - t')$, with $N_j(\omega_j) = [\exp(\hbar\omega_j/k_B T) - 1]^{-1}$ being the equilibrium mean thermal excitation number of the mode j , and T as the bath temperature.

Since the mode c is strongly driven and due to its excitation-exchange interaction with the mode a , the two polaritons have

large amplitudes $|\langle A_+ \rangle|$, $|\langle A_- \rangle| \gg 1$ at the steady state. This allows us to linearize the nonlinear dispersive interaction around steady-state values. This is implemented by writing each mode operator O , $O = A_+, A_-, b$, as the sum of its classical average and quantum fluctuation operator, i.e., $O = \langle O \rangle + \delta O$, and neglecting small second-order fluctuation terms in Eq. (3). We aim to study quantum entanglement between the two polariton modes, and hence focus on the dynamics of the quantum fluctuations. The quantum fluctuations of the system (δA_+ , δA_- , δb) are governed by the following linearized QLEs:

$$\begin{aligned} \delta\dot{A}_+ &= -(i\Delta_+ + \kappa_+) \delta A_+ - \delta\kappa \delta A_- - G_{+b} \frac{\delta b + \delta b^\dagger}{2} + \sqrt{2\kappa_+} A_+^{in}, \\ \delta\dot{A}_- &= -(i\Delta_- + \kappa_-) \delta A_- - \delta\kappa \delta A_+ - G_{-b} \frac{\delta b + \delta b^\dagger}{2} + \sqrt{2\kappa_-} A_-^{in}, \\ \dot{\delta b} &= -(i\omega_b + \kappa_b) \delta b - G_{+b} \frac{\delta A_+^\dagger - \delta A_+}{2} - G_{-b} \frac{\delta A_-^\dagger - \delta A_-}{2} + \sqrt{2\kappa_b} b^{in}, \end{aligned} \quad (4)$$

where $G_{+b} \equiv G_+ \sin \theta$ ($G_{-b} \equiv G_- \cos \theta$) represents the coupling strength between the polariton A_+ (A_-) and the mode b , with $G_{+-} \equiv G_+ \sin \theta + G_- \cos \theta$, and $G_{\pm} \equiv i2G_0 \langle A_{\pm} \rangle$ being the enhanced dispersive coupling strengths associated with the two polaritons. In obtaining Eq. (4), we neglect the linear coupling terms between the two polaritons $\mathcal{G}(\delta A_+^\dagger \delta A_- + \delta A_+ \delta A_-^\dagger)$, where $\mathcal{G} = G_0 \text{Re} \langle b \rangle \sin 2\theta$, due to their weak strength and negligible impact on the entanglement [30]. Under the optimal conditions for the entanglement $|\Delta_{\pm}| \simeq \omega_b \gg \kappa_{\pm}$ (c.f. Fig. 1(b)), as will be discussed later, we obtain approximate analytical expressions of the steady-state averages, i.e.,

$$\begin{aligned} \langle A_+ \rangle &\simeq \frac{\delta\kappa \Omega \cos \theta - i\Omega \sin \theta (\Delta_- - i\kappa_-)}{(\Delta_- - i\kappa_-)(\Delta_+ - i\kappa_+) + \delta\kappa^2}, \\ \langle A_- \rangle &\simeq \frac{\delta\kappa \Omega \sin \theta - i\Omega \cos \theta (\Delta_+ - i\kappa_+)}{(\Delta_+ - i\kappa_+)(\Delta_- - i\kappa_-) + \delta\kappa^2}, \\ \text{Re} \langle b \rangle &= -\frac{G_0}{\omega_b} |\langle A_+ \rangle \sin \theta + \langle A_- \rangle \cos \theta|^2. \end{aligned} \quad (5)$$

Because of the weak coupling G_0 , the frequency shift caused by the dispersive coupling is typically much smaller than the resonance frequency ω_b , as observed, e.g., in optomechanical [32] and magnomechanical experiments [24–26]. Therefore, in deriving Eqs. (4) and (5) we safely neglect this small frequency shift in the detunings $|\Delta_{\pm}| \simeq \omega_b$.

The QLEs (4) can be expressed using quadratures $(\delta X_{\pm}, \delta Y_{\pm}, \delta X_b, \delta Y_b)$, with $\delta X_{\pm} = (\delta A_{\pm} + \delta A_{\pm}^\dagger)/\sqrt{2}$, $\delta Y_{\pm} = i(\delta A_{\pm}^\dagger - \delta A_{\pm})/\sqrt{2}$, and $\delta X_b = (\delta b + \delta b^\dagger)/\sqrt{2}$, $\delta Y_b = i(\delta b^\dagger - \delta b)/\sqrt{2}$, and be cast in the matrix form of

$$\dot{u}(t) = \mathcal{R}u(t) + n(t), \quad (6)$$

where $u(t) = [\delta X_+(t), \delta Y_+(t), \delta X_-(t), \delta Y_-(t), \delta X_b(t), \delta Y_b(t)]^T$, $n(t) = [\sqrt{2\kappa_+} X_+^{in}, \sqrt{2\kappa_+} Y_+^{in}, \sqrt{2\kappa_-} X_-^{in}, \sqrt{2\kappa_-} Y_-^{in}, \sqrt{2\kappa_b} X_b^{in}, \sqrt{2\kappa_b} Y_b^{in}]^T$,

and the drift matrix \mathcal{R} is given by

$$\mathcal{R} = \begin{pmatrix} -\kappa_+ & \Delta_+ & -\delta\kappa & 0 & -\text{Re } G_{+b} & 0 \\ -\Delta_+ & -\kappa_+ & 0 & -\delta\kappa & -\text{Im } G_{+b} & 0 \\ -\delta\kappa & 0 & -\kappa_- & \Delta_- & -\text{Re } G_{-b} & 0 \\ 0 & -\delta\kappa & -\Delta_- & -\kappa_- & -\text{Im } G_{-b} & 0 \\ 0 & -\text{Im } G_{+b} & 0 & -\text{Im } G_{-b} & -\kappa_b & \omega_b \\ 0 & \text{Re } G_{+b} & 0 & \text{Re } G_{-b} & -\omega_b & -\kappa_b \end{pmatrix}. \quad (7)$$

Since the quantum noises are Gaussian and the system dynamics is linearized, the steady state of the quadrature fluctuations is a continuous-variable three-mode Gaussian state, which can be completely characterized by a 6×6 covariance matrix (CM) V with its entries defined as $V_{ij} = \frac{1}{2}\langle u_i(t)u_j(t') + u_j(t')u_i(t) \rangle$ ($i, j = 1, 2, \dots, 6$). The steady-state CM V can be achieved by solving the Lyapunov equation [33]

$$\mathcal{R}V + V\mathcal{R}^T = -D, \quad (8)$$

where $D = \text{Diag}[\kappa_+(2N_+ + 1), \kappa_+(2N_+ + 1), \kappa_-(2N_- + 1), \kappa_-(2N_- + 1), \kappa_b(2N_b + 1), \kappa_b(2N_b + 1)]$ is the diffusion matrix, which is defined via $D_{ij}\delta(t - t') = \langle n_i(t)n_j(t') + n_j(t')n_i(t) \rangle/2$. The mean thermal excitation numbers N_{\pm} are related to N_a and N_c via $N_+ = \{[\kappa_a \cos^2 \theta(2N_a + 1) + \kappa_c \sin^2 \theta(2N_c + 1)]/\kappa_+ - 1\}/2$ and $N_- = \{[\kappa_a \sin^2 \theta(2N_a + 1) + \kappa_c \cos^2 \theta(2N_c + 1)]/\kappa_- - 1\}/2$. We adopt the logarithmic negativity E_N [34] to quantify the entanglement between the two polaritons, which is defined based on the 4×4 CM V_4 of the two polariton modes (V_4 is extracted by removing irrelevant rows and columns in V). Specifically, $E_N = \max[0, -\ln(2\eta^-)]$, where $\eta^- \equiv 2^{-1/2}[\Sigma - (\Sigma^2 - 4 \det V_4)^{1/2}]^{1/2}$, and $V_4 = [V_+, V_{+-}; V_{+-}^T, V_-]$, with V_+ , V_- and V_{+-} being the 2×2 blocks of V_4 , and $\Sigma \equiv \det V_+ + \det V_- - 2\det V_{+-}$.

Entanglement of two polaritons.—The mechanism of creating entanglement between the two polaritons is as follows. The mode b scatters the driving field at frequency ω_0 onto two sidebands at $\omega_0 \pm \omega_b$ (see Fig. 1(b)). When the frequencies of the two polaritons are adjusted to be resonant with the two sidebands, i.e., $\Delta_+ = -\Delta_- \simeq \omega_b$, both the Stokes and anti-Stokes scatterings are effectively activated, where the Stokes scattering corresponds to the PDC interaction causing the lower-frequency polariton to be entangled with the mode b , while the anti-Stokes scattering leads to the state-swap (beam-splitter) interaction between the higher-frequency polariton and the mode b . Therefore, the two polaritons get entangled via the mediation of the mode b when the above two processes are simultaneously activated.

The interactions between the polaritons and the mode b essentially result from the dispersive coupling between the mode b and the component of the mode c in the polaritons. Therefore, by varying the weight of the mode c in the polaritons (via altering θ), one can adjust the *effective* strength of the PDC (state-swap) interaction associated with the Stokes (anti-Stokes) scattering. For the special case $\theta = \frac{\pi}{4}$, $\theta \in [0, \frac{\pi}{2}]$, where both the polaritons A_{\pm} have equally weighted modes a and c , the strengths of the Stokes and anti-Stokes scatterings are equal. This point easily causes the system to be unstable

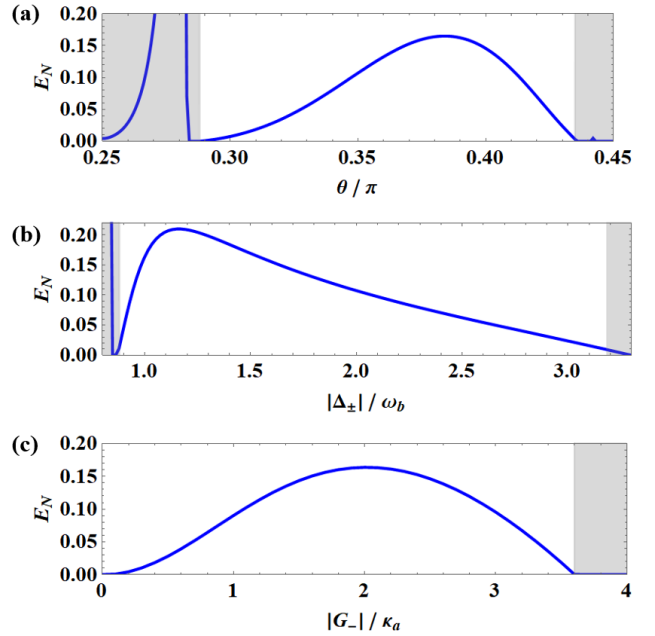


FIG. 2: Stationary entanglement between two polaritons E_N versus (a) θ ; (b) the polariton-drive detuning $|\Delta_{\pm}|$; (c) the coupling strength $|G_-|$. We take $|G_-|/2\pi = 2$ MHz and $\Delta_+ = -\Delta_- = \omega_b$ in (a). The parameters of (b) ((c)), apart from Δ_{\pm} ($|G_-|$), correspond to those yielding an optimal angle $\theta = 0.38\pi$ in (a). The grey areas denote the regimes where the system is unstable. See text for other parameters.

(c.f. Fig. 2(a)) and only nonstationary entanglement could be produced [35]. Therefore, a larger $\theta > \frac{\pi}{4}$ should be considered to obtain stationary entanglement, where the anti-Stokes scattering (cooling) outperforms the Stokes scattering (amplification). For a relatively small value of θ , e.g., $\theta < \frac{\pi}{3}$, we find that the entanglement between the two polaritons is small, while the entanglement between the lower-frequency polariton A_- and the mode b is strong. This indicates that the entanglement (A_- & b) is effectively generated by the Stokes scattering, but is not yet efficiently transferred to the higher-frequency polariton A_+ . The state-swap interaction between the polariton A_+ and the mode b in the anti-Stokes scattering should thus be enhanced. To this end, we further increase θ in order to raise the weight of the mode c in the polariton A_+ , which enhances the strength of the anti-Stokes scattering. Consequently, we see an efficient entanglement transfer and the two polaritons are strongly entangled around $\theta \simeq 0.38\pi$, as clearly shown in Fig. 2(a). However, θ cannot be too large (i.e., too close to $\frac{\pi}{2}$), as this reduces the weight of the mode c in the polariton A_- and thus the strength of the associated Stokes scattering, from which the entanglement of the system originates. Therefore, an optimal θ exists for the entanglement as the result of the trade-off between the strengths of the Stokes and anti-Stokes scatterings, as seen in Fig. 2(a).

As an example to demonstrate our mechanism, Fig. 2 is plotted with the parameters of a cavity magnomechanical system [9, 24–26]. It consists of two strongly-coupled bosonic modes: a microwave cavity (a) and a magnon (c) mode form-

ing two polaritons [13–15] (typically in gigahertz), and a mechanical vibration mode (b , in megahertz) that is coupled to the magnon mode via a dispersive magnetostrictive interaction. Note that the magnon mode is bosonized under the condition of low-lying excitations [36]. We adopt experimentally feasible parameters [24–26]: $\omega_a/2\pi = 10$ GHz, $\omega_b/2\pi = 10$ MHz, $\kappa_a/2\pi = \kappa_c/2\pi = 1$ MHz, $\kappa_b/2\pi = 100$ Hz, and at low temperature $T = 10$ mK. We further consider the optimal detunings $\Delta_+ = -\Delta_- = \omega_b$ in Fig. 2(a), as analyzed above. For a given θ , g and ω_c can be determined by solving the equations $\theta = \frac{1}{2} \arctan \frac{2g}{\omega_a - \omega_c}$ and $\sqrt{(\omega_a - \omega_c)^2 + 4g^2} = 2\omega_b$ ($\omega_{a,b}$ are assumed constant). We note that the magnon frequency ω_c and the cavity-magnon coupling strength g can be readily adjusted by varying the bias magnetic field and the position of the ferromagnet inside the microwave cavity, respectively [13–15]. The stability of the system is guaranteed by the negative eigenvalues (real parts) of the drift matrix \mathcal{R} . We find that, apart from the unstable region when θ is small ($\theta < 0.29\pi$), the system can also be unstable when θ is too large. This is because the coupling strength $|G_+|$ (associated with the polariton A_+) increases rapidly as θ grows, $\theta \rightarrow \frac{\pi}{2}$, due to the relation $|G_+| \simeq \tan \theta$ ($|G_-|$ is fixed in Fig. 2(a)).

An optimal $\theta \simeq 0.38\pi$ gives the maximum entanglement in Fig. 2(a), which corresponds to $g/2\pi \simeq 6.85$ MHz and $\omega_c/2\pi \simeq 10.0146$ GHz. To investigate the effect of the deviation of the polaritons from the mechanical sidebands, we change ω_c in Fig. 2(b) to vary the polariton frequencies (i.e., Δ_{\pm}). Specifically, we set the drive frequency $\omega_0 = \frac{\omega_a + \omega_c}{2}$, which ensures two symmetric polaritons ($\Delta_+ = |\Delta_-|$) and mechanical sidebands with respect to the drive frequency. It shows that when the two polaritons deviate from the two mechanical sidebands ($|\Delta_{\pm}|$ away from ω_b), the entanglement reduces, confirming our earlier analysis on the optimal condition $\Delta_+ = -\Delta_- \simeq \omega_b$ for the entanglement. The unstable region on the left of Fig. 2(b) is due to the fact that a small $|\Delta_{\pm}|$ corresponds to a small θ , and thus a weak strength of the anti-Stokes scattering (cooling process). The unstable region on the right is because that a large $|\Delta_{\pm}|$ corresponds to θ approaching $\frac{\pi}{2}$, and thus a large value of $|G_+|$. This is similar to the reason of instability on the right side of Fig. 2(a).

In Fig. 2(c), we plot the entanglement versus the effective coupling rate G_- . Clearly, as $|G_-|$ grows the entanglement reaches its maximum in the stable regime and then reduces before entering the unstable regime. This means that one can obtain the maximum entanglement *in the stable regime*, and the maximum entanglement is no longer constrained by the stability condition [33, 37]. This implies that the entanglement mechanism presented here fundamentally differs from those in the protocols of, e.g., Refs. [9, 33].

It should be noted that the results of Fig. 2 are obtained under the condition of $\kappa_a \simeq \kappa_c$. For the case of $\delta\kappa$ being comparable to or larger than $\kappa_{a(c)}$, the associated coupling terms between the two polaritons (c.f. Eq. (4)) may have a significant impact on the entanglement. In Fig. 3(a), we plot the entanglement versus the two dissipation rates κ_a and κ_c . It shows that

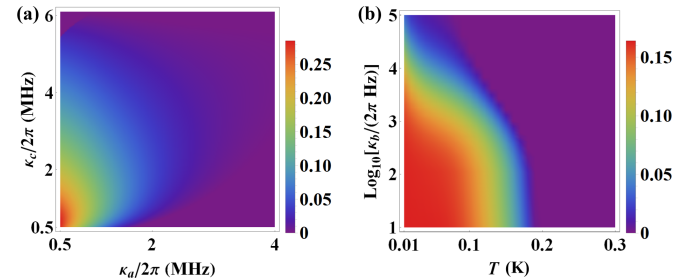


FIG. 3: Stationary polariton entanglement E_N versus (a) dissipation rates κ_a and κ_c ; (b) bath temperature T and κ_b . We take $\theta = 0.38\pi$, and the other parameters are the same as in Fig. 2(a).

for a wide range of $\kappa_{a(c)}$, the entanglement is present. The entanglement is also robust with respect to the bath temperature T and the mechanical damping rate κ_b , as shown in Fig. 3(b). The entanglement survives for the temperature up to $T \sim 180$ mK (κ_b up to $\sim 2\pi \times 10^5$ Hz), under experimentally feasible parameters.

Conclusion and discussion.—The presented entanglement theory can be applied to many different bosonic systems. The system contains two strongly-coupled bosonic modes and a third mode that dispersively couples to one of the strongly-coupled modes. The mechanism can be exploited to entangle two gigahertz cavity-magnon polaritons in cavity magnomechanics by introducing the dispersive magnetostrictive coupling to a megahertz vibration phonon mode, as illustrated above. It is also promising to entangle exciton-photon polaritons in the exciton-optomechanics system [27–29], where excitons and photons are strongly coupled in a microcavity. Similarly, one can also entangle plasmon-photon polaritons [19] in the plasmon-photon-phonon system, where the photons couple to vibration phonons via a dispersive interaction (e.g., via radiation pressure [32]). Essentially, any other bosonic systems governed by the Hamiltonian (1) could prepare two strongly-entangled hybridized modes. The mechanism optimally works in the resolved-sideband limit, and therefore the dissipation rates of the polariton modes should be smaller than the resonance frequency of the third mode.

To conclude, we present a general mechanism of entangling two strongly-coupled bosonic modes by introducing a third dispersively-coupled mode. The presence of the third mode activates the PDC and the state-swap interactions associated with the two hybridized modes, which become entangled when the strengths of the two interactions are properly chosen. We discuss on how to apply the mechanism to a variety of three-mode bosonic systems. The work would find promising applications in various quantum tasks requiring bosonic entangled states, and in the study of macroscopic quantum states.

Acknowledgments.—This work has been supported by Zhejiang Province Program for Science and Technology (Grant No. 2020C01019) and the National Natural Science Foundation of China (Grant No. 11874249).

* jiel007@zju.edu.cn

[1] A. Furusawa, J. L. Sorensen, S. L. Braunstein, C. A. Fuchs, H. J. Kimble, E. S. Polzik, *Science* **282**, 706 (1998).

[2] H. J. Kimble, *Nature* **453**, 1023 (2008).

[3] V. Giovannetti, S. Lloyd, L. Maccone, *Nat. Photon.* **5**, 222 (2011).

[4] X. Li, Q. Pan, J. Jing, J. Zhang, C. Xie, and K. Peng, *Phys. Rev. Lett.* **88**, 047904 (2002).

[5] S. L. Braunstein and P. van Loock, *Rev. Mod. Phys.* **77**, 513 (2005).

[6] R. Horodecki, P. Horodecki, M. Horodecki, and K. Horodecki, *Rev. Mod. Phys.* **81**, 865 (2009).

[7] C. F. Ockeloen-Korppi *et al.*, *Nature* **556**, 478 (2018).

[8] S. Kotler *et al.*, *Science* **372**, 622 (2021).

[9] J. Li, S.-Y. Zhu, and G. S. Agarwal, *Phys. Rev. Lett.* **121**, 203601 (2018).

[10] J. Li and S.-Y. Zhu, *New J. Phys.* **21**, 085001 (2019).

[11] A. Bassi, K. Lochan, S. Satin, T. P. Singh, and H. Ulbricht *Rev. Mod. Phys.* **85**, 471 (2013).

[12] F. Fröwis, P. Sekatski, W. Dür, N. Gisin, and N. Sangouard, *Rev. Mod. Phys.* **90**, 025004 (2018).

[13] H. Huebl, C.W. Zollitsch, J. Lotze, F. Hocke, M. Greifenstein, A. Marx, R. Gross, and S. T. B. Goennenwein, *Phys. Rev. Lett.* **111**, 127003 (2013).

[14] Y. Tabuchi, S. Ishino, T. Ishikawa, R. Yamazaki, K. Usami, and Y. Nakamura, *Phys. Rev. Lett.* **113**, 083603 (2014).

[15] X. Zhang, C. L. Zou, L. Jiang, and H. X. Tang, *Phys. Rev. Lett.* **113**, 156401 (2014).

[16] H. Deng, H. Haug, and Y. Yamamoto, *Rev. Mod. Phys.* **82**, 1489 (2010).

[17] C. Weisbuch, M. Nishioka, A. Ishikawa, and Y. Arakawa *Phys. Rev. Lett.* **69**, 3314 (1992).

[18] D. G. Lidzey, D. D. C. Bradley, M. S. Skolnick, T. Virgili, S. Walker, and D. M. Whittaker, *Nature* **395**, 53 (1998).

[19] D. G. Baranov *et al.*, *Nat. Commun.* **11**, 2715 (2020).

[20] J. Bellessa, C. Bonnand, J. C. Plenet, and J. Mugnier, *Phys. Rev. Lett.* **93**, 036404 (2004).

[21] Y. Sugawara, T. A. Kelf, J. J. Baumberg, M. E. Abdelsalam, and P. N. Bartlett, *Phys. Rev. Lett.* **97**, 266808 (2006).

[22] G. Zengin, M. Wersäll, S. Nilsson, T. J. Antosiewicz, M. Käll, and T. Shegai, *Phys. Rev. Lett.* **114**, 157401 (2015).

[23] R. Liu *et al.*, *Phys. Rev. Lett.* **118**, 237401 (2017).

[24] X. Zhang, C.-L. Zou, L. Jiang, and H. X. Tang, *Sci. Adv.* **2**, e1501286 (2016).

[25] C. A. Potts, E. Varga, V. Bittencourt, S. V. Kusminskiy, and J. P. Davis, *Phys. Rev. X* **11**, 031053 (2021).

[26] R.-C. Shen, J. Li, Z.-Y. Fan, Y.-P. Wang, and J. Q. You, *Phys. Rev. Lett.* **129**, 123601 (2022).

[27] O. Kyriienko, T. C. H. Liew, and I. A. Shelykh, *Phys. Rev. Lett.* **112**, 076402 (2014).

[28] B. Jusserand, A. N. Poddubny, A. V. Poshakinskiy, A. Fainstein, and A. Lemaitre, *Phys. Rev. Lett.* **115**, 267402 (2015).

[29] N. Carlon Zambon, Z. Denis, R. De Oliveira, S. Ravets, C. Ciuti, I. Favero, and J. Bloch, *Phys. Rev. Lett.* **129**, 093603 (2022).

[30] See Supplemental Material for additional proofs.

[31] C.W. Gardiner and P. Zoller, *Quantum Noise* (Springer, Berlin, 2000).

[32] M. Aspelmeyer, T. J. Kippenberg, and F. Marquardt, *Rev. Mod. Phys.* **86**, 1391 (2014).

[33] D. Vitali *et al.*, *Phys. Rev. Lett.* **98**, 030405 (2007).

[34] G. Vidal and R. F. Werner, *Phys. Rev. A* **65**, 032314 (2002); G. Adesso, A. Serafini, and F. Illuminati, *Phys. Rev. A* **70**, 022318 (2004); M. B. Plenio, *Phys. Rev. Lett.* **95**, 090503 (2005).

[35] J. Li, I. Moaddel Haghghi, N. Malossi, S. Zippilli, and D. Vitali, *New J. Phys.* **17**, 103037 (2015).

[36] D. Lachance-Quirion, Y. Tabuchi, A. Gloppe, K. Usami, and Y. Nakamura, *Appl. Phys. Express* **12**, 070101 (2019).

[37] S. G. Hofer, W. Wieczorek, M. Aspelmeyer, and K. Hammerer, *Phys. Rev. A* **84**, 052327 (2011).